ASTROPHYSICS AND SPACE SCIENCE LIBRARY 355

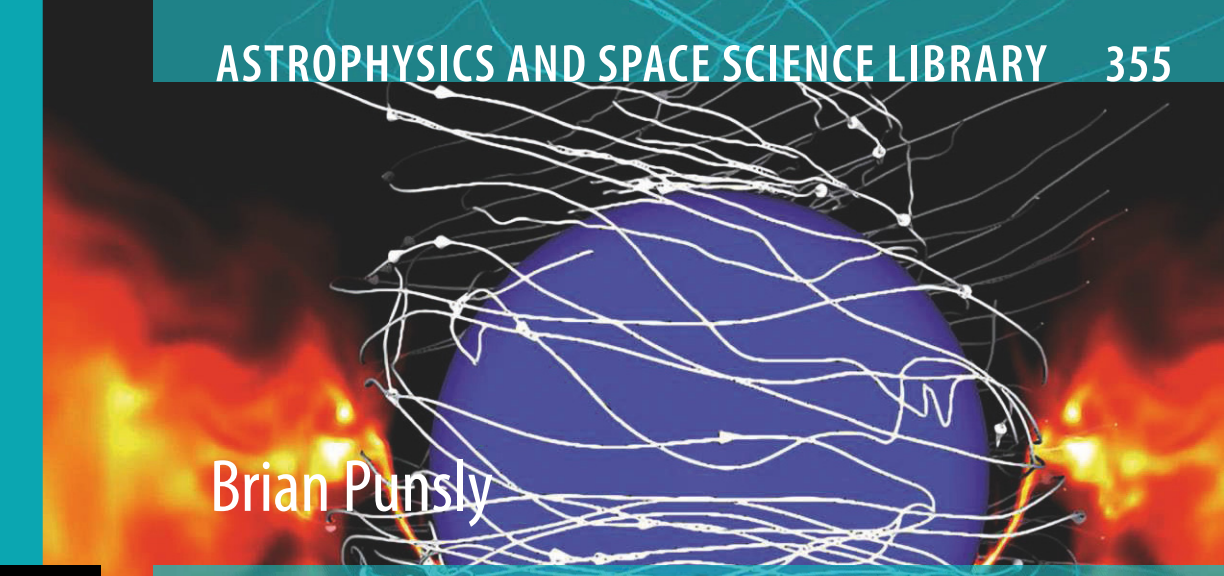

Brian Punsly

# Black Hole Gravito-hydromagnetics

2nd Edition

ASSL

Springer

# Black Hole Gravitohydromagnetics

# Astrophysics and Space Science Library

# Black Hole Gravitohydromagnetics

## Second Edition

*by*

Brian Punsly

Springer

Brian Punsly
4014 Emerald St. 116
Torrance, CA
USA
and
ICRANet
Piazza della Repubblica 10
65100, Pescara
Italy

Cover Illustration: A plot of the magnetic field (the white curves) around a rapidly rotating black hole (the blue disk) in a 3-D MHD numerical simulation called "KDJ" that is discussed in detail in Chapter 11 (at time step 10,000 M in geometrized units). The false color contour plot depicts the density of turbulent accreting gas. The gravito-hydromagnetic dynamo (the subject of this book), in the inner regions of the accretion flow, twists the magnetic field azimuthally. These rotating magnetic twists propagate vertically as powerful, bipolar jets of electromagnetic energy (Poynting flux). This plot was provided courtesy of Shigenobu Hirose using the freeware, Paraview. Note that the North and South poles in the Paraview plot are reversed relative to the plots in Chapter 11, therefore the stronger jet is in the Northern hemisphere.

ISBN: 978-3-540-76955-2 e-ISBN: 978-3-540-76957-6
DOI: 10.1007/978-3-540-76957-6

Library of Congress Control Number: 2008929587



*Cover design*: eStudio Calamar S.L.

Printed on acid-free paper

9 8 7 6 5 4 3 2 1

springer.com

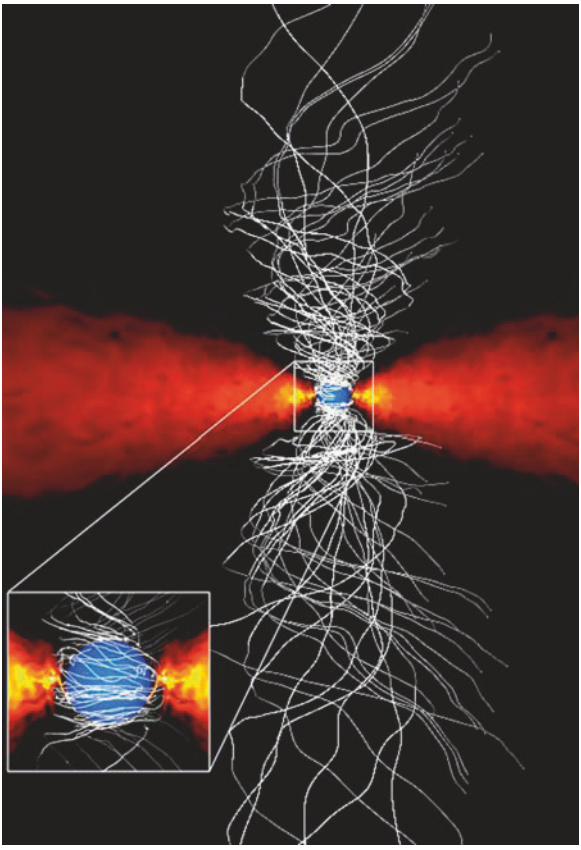

A plot of the magnetic field (the white curves) around a rapidly rotating black hole (the blue disk) in a 3-D MHD numerical simulation called "KDJ" that is discussed in detail in Chapter 11 (at time step 10,000 M in geometrized units). The false color contour plot depicts the density of turbulent accreting gas. This is an expanded view of the cover illustration (in the inset) that highlights the large scale relativistic bipolar jets that are driven by the gravitohydromagnetic dynamo. The low pitch angle magnetic helices in the outer regions of the nested set of field lines correspond to the regions of strongest Poynting (electromagnetic energy) flux in the jet. A strong flare is just beginning in the Southern hemisphere. Note that the North and South poles in the Paraview plot are reversed relative to the plots in Chapter 11. This plot was provided courtesy of Shigenobu Hirose.

# Preface

"Black hole gravitohydromagnetics," or simply black hole GHM, is the study of the physical interactions of highly magnetized plasmas in the context of the differential spacetime rotation (known colloquially as the dragging of inertial frames) that is induced by the gravitational field of a rapidly rotating (Kerr) black hole. The strong large-scale magnetic field limit is essential for the external Universe to be significantly coupled to the black hole. In fact, it allows for a physical realization of the Christodoulou/Ruffini or Penrose/Floyd conceptualizations of black hole energy extraction. This is a concept that is often abused in the astrophysical community as most processes that torque a black hole only do so if the internal energy of the black hole is increased as well. A true "Penrose process" actually decreases the internal energy of the black hole. This tight constraint on the inflowing plasma state is fundamental to black hole GHM. It is the ability of GHM to describe the underlying physics behind the extraction of rotational inertia from a black hole that is of interest in astronomy. Specifically, the relevance of supermassive black hole central engines in powerful extragalactic radio sources is strongly suggested by the most modern observational evidence that is presented in Chapters 1 and 10. The theory is likely applicable to galactic black holes and "collapsars" in certain circumstances that have yet to be explored.

The main advances in the study of GHM since the first edition of this book are the advent of perfect magnetohydrodynamic simulations of black hole magnetospheres. Chapter 11 is a study of numerical simulations performed during the last seven years that are relevant to GHM. All theoretical treatments of black hole driven jets of plasma are predicated on certain assumptions. The most significant of these is the poloidal magnetic field distribution in the black magnetosphere. The bottom line on this topic is that we still know very little about what the magnetic field "usually" looks like around a supermassive black hole in an active galactic nucleus. For example, the ergospheric disk in Chapter 8 of this book assumes a large scale vertical magnetic flux in the equatorial plane near the black hole event horizon in the ergosphere. So far, no simulation has shown this to occur; however, only a very small subset of the astrophysically possible magnetospheric environments have been explored to date. The simulations can teach us about new possibilities that were not

previously envisioned. For example, it was surprising to see that a strong GHM interaction in 3-D simulations drives powerful, episodic flares of relativistic plasma from the ergospheric accretion flow near the equatorial plane. In a time averaged sense, the GHM driven flares mimic many of the fundamental features of the idealized ergospheric disk. The flares of electromagnetic energy flux are coincident with flares in vertical magnetic flux that permeate the inner regions of the ergospheric equatorial accretion flow. The random local plasma physics that produces these flares in vertical flux is the ultimate trigger for the GHM driven jets. In summary, the simulations teach us about field configurations that were never before visualized. Since the poloidal magnetic flux distribution near a supermassive black hole is not known, this is fertile ground for expanding our understanding of black hole driven jets. It is likely that this will be the focal point of most numerical work in the near future.

A massive endeavor like the second edition of this book does not happen in isolation. I wish to thank Jean-Pierre DeVilliers, John Hawley and Julian Krolik for sharing their state of the art 3-D simulations of black hole accretion flows. These were extensive supercomputing efforts involving many hundreds of CPUs. I would never have been able to generate one of these complex numerical simulations and I am lucky that they were generous with their knowledge and data. I am also indebted to Vladimir Semenov and Sergey Dyadechkin who, working tirelessly with a small 2 GHz processor, generated the beautiful movies of the GHM interaction and subsequent jet production for Science magazine. These results are summarized in Section 11.2. Finally, this effort was facilitated by the support of ICRANET over the years. They have supported the page charges for the numerous peer reviewed papers that led to this second edition. The intellectual support and friendship of Remo Ruffini has been instrumental in the long-term pursuit of these topics.

Los Angeles, July 2008 *Brian Punsly*

# Contents

# Chapter 1
# Introduction

## 1.1 Introductory Physical Perspective

The importance of magnetized plasma in astrophysical objects manifests itself in a wide range of phenomena from solar flares and the Aurora Borealis to pulsar winds and extragalactic radio jets. It is now widely accepted that 1–20$M_\odot$ black holes populate the galaxies that fill the Universe. Furthermore, water maser mappings with the VLBA (Very Long Baseline Array) and kinematical gas analysis with HST (The Hubble Space Telescope) make a convincing argument that central black holes in galaxies are commonplace with masses of $10^5 M_\odot$ to more than $10^9 M_\odot$ (for a good review of these data see [1,2]). Thus, one expects that the interactions of magnetized plasma with the gravitational fields of black holes permeate the Universe and the astrophysical consequences should be spectacular. This monograph is the first text designed to be a formal study of this new branch of physics which is such a fundamental part of our Universe.

Why a new branch of physics? Fluid mechanics is well described by hydrodynamics. However, the introduction of magnetic fields into the flow of fluids, gases and plasmas creates forces unknown to hydrodynamics. This produces a much higher level of complexity requiring the development of a new subject, magnetohydrodynamics (MHD), or as it is sometimes called, hydromagnetics. Similarly, plasmas interacting with both magnetic fields and the near field gravitational forces of a black hole are an order of magnitude more complex than pure MHD flows. Consequently, a new formalism is required that synthesizes general relativity and plasma physics. In particular, we are interested in plasma effects induced by black hole gravity that cannot be found in more commonly studied astrophysical environments. For example, accretion disks could be found around any compact object. The combination of both magnetic and gravitational interactions with plasma flows is encompassed in the expression gravitohydromagnetics (GHM).

This is neither an easy subject to present nor to be absorbed by the student or reader. The interaction is reasonably complex by physical standards; however, the real impediment is that the subject spans two disparate areas of physics. Relativists are typically uncomfortable with the sophisticated plasma physics required to

B. Punsly, *Black Hole Gravitohydromagnetics, 2nd. ed.*,
Astrophysics and Space Science Library 355, doi: 10/1007/978-3-540-76957-6_1,

describe the dynamical response of a magneto-fluid to the immense gravitational force applied by a black hole. Similarly, astrophysicists, who are well versed in standard plasma calculations, are generally unfamiliar with the advanced level of relativistic formalism necessary to probe the underlying physical interaction. This book unfortunately compromises on the review of background material for the sake of cogency. As such, a reader who has not taken a course in general relativity most likely will be overwhelmed and may never appreciate the rigorous nature of many of the basic physical concepts presented.

In spite of historical efforts to simplify the subject, the dynamics of accreting plasma in strong magnetic fields near a black hole are far from trivial. The existence of two strong forces (electromagnetic and gravitational) is incompatible with a simple description of either the plasma being in a perfect MHD state (vanishing proper electric field) everywhere or flowing along geodesic trajectories of the gravitational field. This incompatibility is manifest in the notion that an accreting flow that is dominated by strong magnetic fields (perfect MHD) in the vicinity of the hole must eventually transition to a flow state determined entirely by the gravitational field as it propagates even closer to the event horizon. This dramatic change in character of the flow does not happen gracefully and it is likely to be one of the most intense interactions attainable in the known Universe. The goal of this treatment is to supply the tools (black hole GHM) necessary for developing an intuition for the role of the black hole in this significant astrophysical context. Astrophysically, the most interesting consequence of black hole GHM is the possibility that a wind of magnetized plasma (a jet) can be driven by the interaction of the black hole gravitational field and a plasma filled magnetosphere. The main purpose of this book is to illustrate, through simplified models, the fundamental physical process that allows a rotating black hole to power a magnetized wind.

## 1.2 Evidence for Astrophysical Black Holes

A black hole has never been seen directly by definition. Yet, it is commonly accepted that astrophysical black holes exist. Black holes are "seen" only indirectly through their interactions with nearby matter. Because the gravitational field of a black hole is the most intense of any compact object, one expects unique signatures of their effects on the surrounding environment. For more than two decades, astronomers have been detecting what appears to be the physical manifestations of these theoretically predicted effects.

The most basic reasoning suggests that there is no known subatomic physics that can prevent a large enough mass from catastrophically collapsing to a black hole. The discovery of asymptotic freedom in Quantum Chromodynamics showed that as baryonic matter becomes more compressed, the interaction between constituent quarks becomes weaker (they essentially become Feynman's partons). Thus, our most advanced knowledge of particle physics implies the inevitability of catastrophic collapse through an event horizon if the gravitationally bound mass is large

enough in a collapsing star. Of course, there could be unknown physics that could provide a positive pressure in condensed matter, halting the collapse, but it does not show up in experiments to date.

Based on this, the first evidence for black holes was a direct consequence of the maximum mass allowable for neutron stars (values $\sim$2–3 $M_\odot$ are typically estimated). Beyond this maximum mass, a stellar remnant cannot be supported by degeneracy pressure and collapse to a black hole is inevitable. Thus, the discovery of invisible companions in binary stellar systems with dynamical masses (mass functions) greater than $3\,M_\odot$ was the first evidence for black holes. To date, approximately two dozen black hole candidates are known in binary systems [3, 4].

Clearly, the most famous black hole candidate is Cygnus X-1. It possesses the first predicted indirect feature of a black hole's interaction with surrounding gas. As gas is sucked into a black hole from far away, it gets crammed into smaller volumes. The viscous friction of the accreting gas should produce large amounts of heating and thermal radiation, as modified by electron scattering (see [5] for a discussion of Schwarzschild black holes and [6] for a discussion that includes Kerr black holes). For a black hole of a few solar masses, the thermal temperature of the accreting gas should be very high compared to O-stars. In fact, Cygnus X-1 was discovered by detecting this predicted X-ray emission.

In order to differentiate the spectrum of radiation emanating from accretion as to whether it originates near a black hole or neutron star requires the subjective parametric modeling of the flow. A more convincing argument that differentiates black hole accretion from neutron star accretion has been provided in the context of compact sources that are transient emitters of X-rays and $\gamma$-rays. Differences have been noted in quiescent states produced by advection dominated accretion [7]. For a black hole, the accreting gas must eventually approach the event horizon. Thus, the thermal energy is trapped in the advection dominated flow and becomes redshifted away and the flare ends in a whimper. For a neutron star, the accretion flow terminates on the stellar surface. Thus, the flare can end in a bang of thermonuclear burning or, at a minimum, the thermal energy in the advection dominated flow must be radiated from the heated up star. Consequently, the post flare quiescent states in black holes (transients from compact objects with masses $>3\,M_\odot$) have been observed to be much fainter than for neutron stars [7].

The next strongest circumstantial case for black holes is in the nuclei of galaxies. By observing the kinematics of nuclear gas and stars (by means of the Doppler shift), one can find evidence of simple Keplerian motion in some objects. This provides a straightforward dynamical estimate of the central mass [1]. The greater the spatial resolution, the more convincing the central black hole estimate. The greatest resolution is with high frequency very long baseline interferometry (VLBI). Water maser mappings at 22 GHz with the VLBA resolve subparsec scale structures orbiting the nuclei of nearby galaxies. A handful of mass estimates have been made for central black holes in nearby galaxies [2]. Most of these have insufficient data or an ambiguous interpretation. One measurement is clearly representative of a thin disk with a small warp. Molecular gas appears to be spiralling about a $4.2 \times 10^7\,M_\odot$ black hole in NGC 4258.

**Table 1.1** Dynamically estimated central black hole masses

| Source | Type | $M_{BH}$ ($M_\odot$) | Method |
|---|---|---|---|
| Milky Way | Sbc | $2.8 \times 10^6$ | SD = stellar dynamics |
| NGC 0221 (M 32) | E2 | $3.4 \times 10^6$ | SD |
| NGC 0224 (M 31) | Sb | $3.0 \times 10^7$ | SD |
| NGC 3115 | S0 | $2.0 \times 10^9$ | SD |
| NGC 3377 | E5 | $1.8 \times 10^8$ | SD |
| NGC 3379 (M 105) | E1 | $6.7 \times 10^7$ | SD |
| NGC 4342 | S0 | $3.0 \times 10^8$ | SD |
| NGC 4486B | E1 | $5.7 \times 10^8$ | SD |
| NGC 4594 (M 104) | Sa | $1.0 \times 10^9$ | SD |
| NGC 4374 (M 84) | E1 | $1.4 \times 10^9$ | GD = gas dynamics |
| NGC 4486 (M 87) | E0 | $3.3 \times 10^9$ | GD |
| NGC 4261 | E2 | $4.5 \times 10^8$ | GD |
| NGC 7052 | E4 | $3.3 \times 10^8$ | GD |
| NGC 6251[a] | E2 | $4.8 \times 10^8$ | GD |
| NGC 1068 (M 77) | Sb | $1.0 \times 10^7$ | MD = maser dynamics |
| NGC 4258 (M 106) | Sbc | $4.2 \times 10^7$ | MD |
| NGC 4945 | Scd | $1.4 \times 10^6$ | MD |

[a] Data from [8]; all other data from [2]

A cruder but similar kinematical analysis involves studying the motion of ionized gas with HST. Clear examples of central disks of gas on the order of 100 pc across have been observed in a few galaxies and numerous black hole masses have been estimated from $10^5$–$10^9\,M_\odot$. Table 1.1 lists various black hole masses determined in nearby galaxies [2] including NGC 6251 [8].

Figure 1.1 shows an HST image of the nucleus of NGC 4261, an E2 galaxy. Note the light from the active nucleus penetrating the center of the disk. Inserts (Fig. 1.2) show a radio jet emanating from the active nucleus. A similar HST image of the central disk in NGC 7052, an E4 radio galaxy, is shown in Fig. 1.3. Note that the jet axes are tied to a central engine axis that is not the same as the axis of the disk of orbiting gas.

The earliest indirect evidence for supermassive black holes in galactic nuclei came from the study of active galactic nuclei (AGN). As with galactic black holes in binary systems, the rapid accretion of gas onto the central black hole in a galaxy will have viscous dissipation and a thermal spectrum as modified by electron scattering, a "modified black body" spectrum. Due to the much larger size of the nuclear black holes, the viscous dissipation occurs on much larger scales, producing more radiation with most of the energy emitted at lower frequency (optical/UV as opposed to X-rays). Based on simplified accretion disk models [6, 9], a blue/UV excess was found in Seyfert I galaxy and quasar spectra indicating accretion onto supermassive black holes [10]. This blue/UV excess or "big blue bump" is an ubiquitous property of quasar spectra. In [11], a sample of Seyfert galaxy and quasar spectra were fit by the emission from accretion disks about central black holes with masses ranging from $10^7\,M_\odot$ to $10^9\,M_\odot$ (compare to the dynamical masses in Table 1.1).

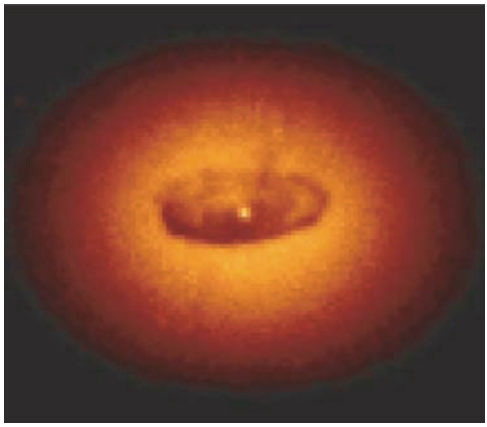

**Fig. 1.1** An HST image of the central disk in the elliptical galaxy NGC 4261. Note the bright central feature, possibly accretion disk radiation from the region of the active nucleus shining through the dusty gaseous disk (alternatively, it could be the high frequency tail of the synchrotron emission form the base of the jet that is shown in Fig. 1.2). The disk is approximately 250 pc across and a gas kinematical estimate of the central black hole mass is $4.5 \times 10^8\,\mathrm{M}_\odot$. Photograph provided courtesy of Laura Ferrarese

To this point we have talked about evidence for black holes through their effect on the nearby environment. In no instance was there cause to invoke magnetized plasma interactions near the hole to explain the data. An interesting case is the class of AGN that are giant elliptical galaxies, often residing at the center of a cluster. These have the most massive central black holes measured to date, $\sim 10^9\,\mathrm{M}_\odot$ (see Table 1.1). They also seem to be the hosts of the radio loud class of AGN as indicated in the examples in Figs. 1.1–1.3 (this seems to hold true for more distant quasars as well [12, 13]). The best studied source of this type is M87, long suspected of harboring a supermassive central black hole. It is not a particularly strong radio source intrinsically, but it is so nearby (in a cosmological sense) that its radio emission can be well studied. It is one of the few radio sources that emits a jet that is optically detected as well. HST images reveal a jet propagating off axis from the center of a disk of nuclear gas on the order of 20 pc in diameter (see Fig. 1.4). Doppler measurements of the disk emission yield a dynamical estimate of a central black hole mass (see Table 1.1). Optically, it appears that the jet is emerging from the environs of the black hole, a finding that is supported by higher resolution radio data as well. The emission from the jet is nonthermal in origin and is well described by synchrotron radiation from hot plasma in a magnetic field that permeates the jet. This is an ubiquitous characteristic of extragalactic radio sources. Astrophysics requires an explanation as to how a jet of magnetized plasma can be generated by the environs of a black hole. The principal application of black hole GHM is the physical explanation of the central engines of extragalactic radio source that it provides.

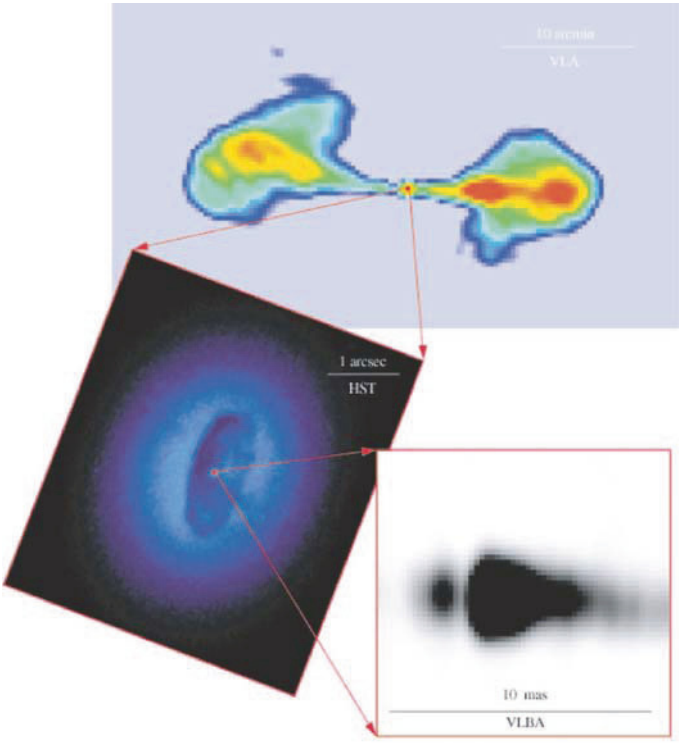


**Fig. 1.2** Inserts of the large scale FR I radio structure of NGC 4261 and the small parsec scale VLBA jet that appears to emanate from the bright spot in the center of the disk (which is featured more prominently in Fig. 1.1). Photograph provided courtesy of Laura Ferrarese

## 1.3 Extragalactic Radio Sources

The most powerful extragalactic radio sources are associated with AGN that produce quasar emission. As stated in the last section, the bright nuclei in AGN are commonly believed to be the light produced by viscous dissipation of an accretion flow onto a black hole. The highest accretion rates produce quasar emission in galactic nuclei. It is estimated in [11] that black holes in quasars accrete mass at a rate sufficient to produce a disk luminosity $L_D > 0.1 L_{Edd}$, where $L_{Edd}$ is the Eddington luminosity at which radiation pressure balances gravity. Seyfert galaxies have accretion rates that are lower, $L_D \sim 0.01 L_{Edd}$, with the most luminous Seyfert galaxies having $L_D \sim 0.1 - 0.2 L_{Edd}$. All of this is model dependent, but it is supported by the few known dynamical black hole mass estimates of AGN as well [14].

A magnetized accretion disk can exist, in principle, around the central black hole of either a Seyfert galaxy or quasar. Theoretically, electrodynamic luminosity (a possible energy source for a jet) is associated with large scale torques applied by a magnetic field and is independent of the gas dynamical viscous losses producing the optical/UV excess comprising the bulk of $L_D$. Thus, if a magnetized accretion

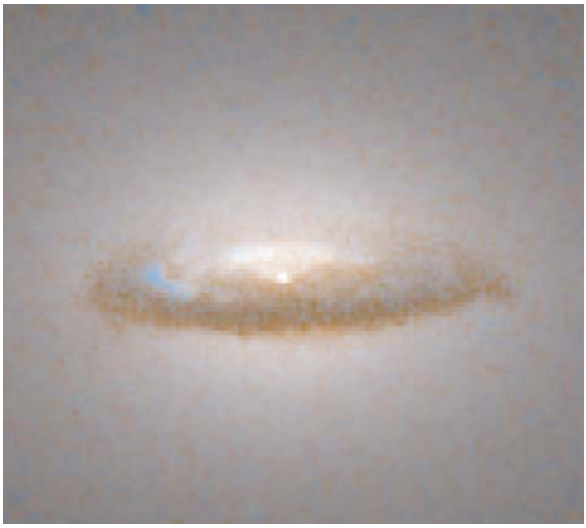

**Fig. 1.3** The central disk of the elliptical galaxy NGC 7052 is revealed in this HST image. The disk is 1,000 pc in diameter and the orbital kinematics imply a central black hole mass of $3 \times 10^8\,M_\odot$. Notice the bright central region that shines through the disk as in NGC 4261. This is a weak radio source and the VLA jet is misaligned with the symmetry axis of the disk, as in NGC 4261. The photograph is provided courtesy of Roeland van der Marel

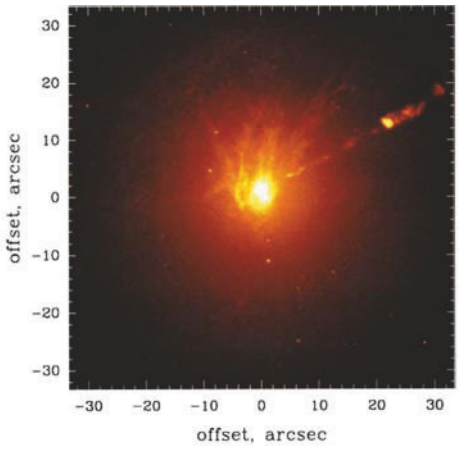


**Fig. 1.4** The optical jet is emanating from the center of the inner disk in this deep HST image of M87. The disk is 20 pc across and the orbital motion indicates a central black hole mass of $3 \times 10^9\,M_\odot$. The photograph is provided courtesy of Holland Ford

disk powers the jet there is no reason why the strongest radio sources should be associated with the highest viscous losses in a flow, quasars.

However, if the quasar phenomenon is associated with the largest influx of angular momentum (largest accretion rates) then one would expect nuclear black holes in quasars to rotate more rapidly in quasars than in Seyfert galaxies or normal galaxies. It is the rotational energy that makes a black hole alive as there is extractable energy or reducible mass [15, 16] (see Sect. 1.4 for a discussion). This suggests the

relevance of rapidly rotating black holes in the central engines of strong extragalactic radio sources.

Furthermore, the accretion flow alone does not seem to power the radio emission as 90% of quasars are radio quiet. The energy radiated from the central engine to the radio lobes can equal or exceed the optical/UV luminosity of a quasar. If accretion powers the radio lobes, then one would expect radio loud quasars to have highly modified accretion with a different optical/UV character than radio quiet quasars. This is contrary to observation. Radio loud quasars have indistinguishable UV broad emission lines, optical/UV luminosities and optical/UV continuum spectra from radio quiet quasars [17, 18]. Note, we did not include all of the optical broad emission lines because of an apparent difference in the optical Fe II complex between radio quiet quasars and lobe dominated radio loud quasars [19]. This strongly suggests that a central engine other than accretion seems to power FR II radio jets and lobes. This is strong circumstantial evidence supporting the hypothesis that black hole energy extraction and GHM is important in these objects.

It seems plausible that the large reducible mass of central black holes in quasars is the reason that the strongest radio sources are powered by the central engine in quasars. Thus, it is the ability of magnetized plasma interactions to extract the rotational energy of a rapidly rotating black hole that is an important application of black hole GHM.

## *1.3.1 Unified Scheme for Radio Loud AGN*

Diagnostics of the central engine can be ascertained by understanding the connections amongst various types of radio loud AGNs. Before the mid-1980s, there appeared to be a zoo of unrelated radio loud AGN morphological types. The interpretation of radio loud AGNs within a unified scheme [20–22] revolutionized our perspective of the central engine (see [23] for a comprehensive review).

Powerful extragalactic radio sources generally occur in one of six categories:

1. FR I (Fanaroff–Riley Type I) radio galaxies
2. FR II radio galaxies
3. Lobe dominated radio loud (FR II) quasars
4. Core dominated radio loud quasars
5. Steep spectrum compact radio cores
6. BL Lac objects

In this section we will briefly describe each class and note its place in the unified scheme.

### 1.3.1.1 FR I Radio Galaxies

FR I radio galaxies have intrinsic extended radio luminosities (integrated from 10 MHz to 250 GHz in the galaxy's rest frame) less than $\sim 10^{43}$ ergs s$^{-1}$ (assuming $H_0 = 55\,\mathrm{km\,s^{-1}\,Mpc^{-1}}$ and $q_0 = 0$ which are used throughout the text un-

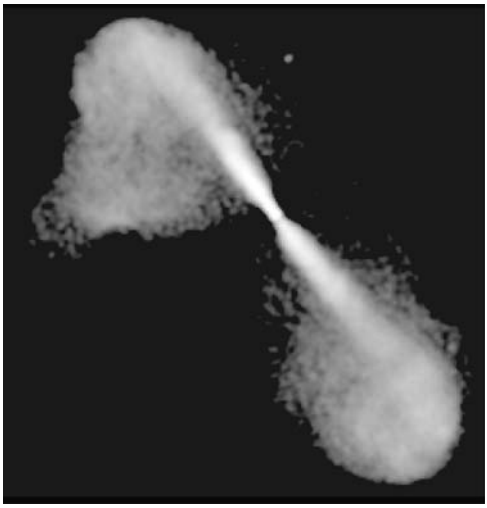

**Fig. 1.5** A 5 GHz deep VLA image of a prototypical FR I radio source 3C 296. The jets are very bright compared to the diffuse lobe emission. Image provided courtesy of Alan Bridle

less otherwise stated). The luminosity is distributed in diffuse plume-like structures extended over a few hundred kiloparsecs. Although there is a wide range of morphologies for FR I radio sources [24], a classical example is given by 3C 296 (see Fig. 1.5). The radio structures in FR I sources do not have concentrated regions of emission called knots and the radio lobes are "edge darkened."

#### 1.3.1.2 FR II Radio Sources

FR II radio galaxies have extended radio luminosities ranging from $10^{43}$ to $10^{47}$ ergs $s^{-1}$. The jets feeding the lobes are more collimated than FR I radio jets on kiloparsec scales. Also, by contrast, most of the radio luminosity emanates from knots in the jet or particularly strong knots in the lobes (called "hot spots") that produce an "edge brightened" appearance. Radio lobes can be separated by distances as large as a few Mpc, implying enormous amounts of stored energy.

Lobe dominated radio loud quasars have lobe and jet luminosities similar to these radio galaxies and are classified as FR II radio sources. Compare the deep VLA maps of the nearby radio galaxy Cygnus A (Fig. 1.6) and the radio loud quasar 3C 175 (Fig. 1.7); the morphology is very similar. FR II quasar counterjet/jet luminosity ratios are significantly less than for FR II radio galaxies. Only one jet is detectable in general, even for the deepest VLA maps (see [25] for a very detailed study). The strongest 3C catalog radio sources tend to be quasars rather than radio galaxies. The main distinction from FR II radio galaxies is the quasar optical/UV emission and broad emission lines from the nucleus. Host galaxy identifications of both FR II radio galaxies and radio loud lobe dominated quasars are always elliptical galaxies or irregular shaped interacting galaxies [13]. This is illustrated in Fig. 1.8 for the FR II radio galaxy 3C 219. Note the strong knot at the base of the counter jet.

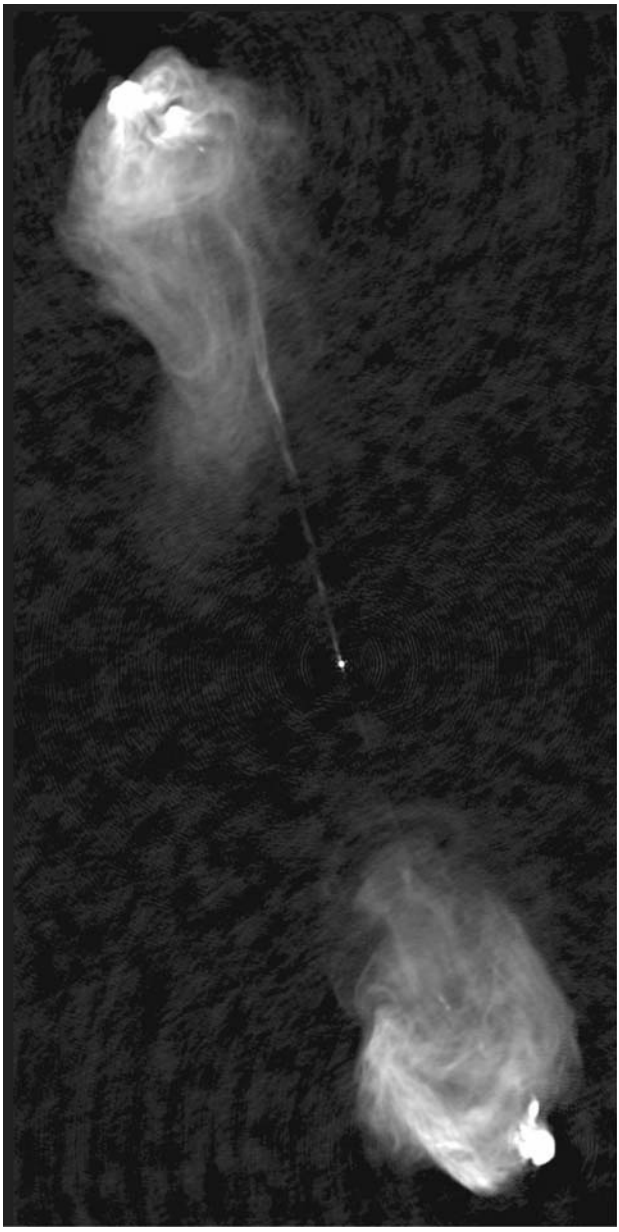

**Fig. 1.6** A deep VLA image of Cygnus A at 5 GHz. The lobes are separated by 180 kpc ($H_0 = 55\,\mathrm{km\,s^{-1}\,Mpc^{-1}}$, $q_0 = 0$). Notice the strong hot spots at the end of each lobe where most of the luminosity resides. A highly collimated low surface brightness jet extends into the eastern lobe from a faint radio core. There are suggestions of a counter jet in the image. The counter jet is more pronounced in Fig. 1.10. The VLA image was provided courtesy of Rick Perley

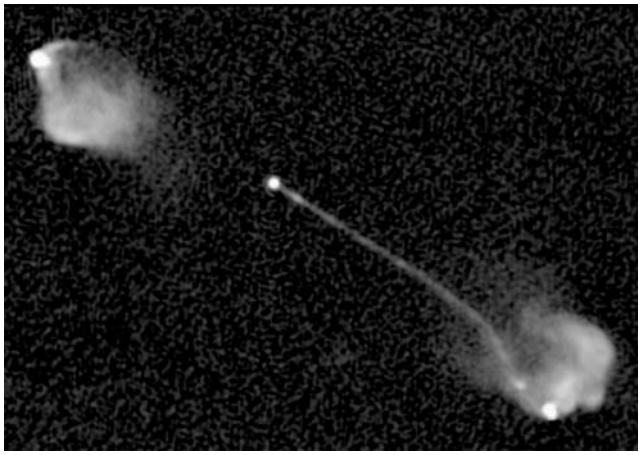

**Fig. 1.7** A deep 5 GHz VLA image of the radio loud quasar 3C 175. Notice the morphological similarity to Cygnus A. The jet is more pronounced relative to the lobe emission than Cygnus A, and there is no hint of a counter jet. This is anecdotal evidence for mildly relativistic flows in kiloparsec scale jets. Image provided courtesy of Alan Bridle

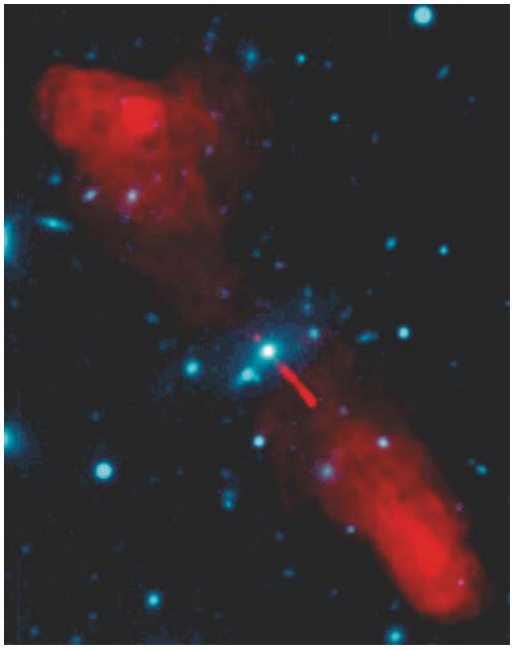

**Fig. 1.8** This deep 5 GHz VLA image of the FR II radio galaxy 3C 219 shows a strong jet and a knot in a counter jet. It is overlaid on the diffuse (blue) optical image of the host elliptical galaxy. Image provided courtesy of Alan Bridle

#### 1.3.1.3 Core Dominated Quasars

Certain quasars have very strong radio cores that appear more dominant at high radio frequency (i.e., 5 GHz or above). The cores are merely unresolved radio jets. Current VLBI imaging at high frequency, 43 and 86 GHz, resolves jets to a fraction of a milliarcsecond. The jets look very similar on all scales from an arcsecond down. Higher resolution always reveals more knots of radio emission in the jet. Most of these core dominated quasars have microwave spectral indices that are much flatter than the steep spectral emission found in lobes. If one defines the spectral flux, $F_\nu$, then a power law often approximates the spectrum in a band of frequencies, $F_\nu = F_0 \nu^{-\alpha}$. For lobes, $\alpha \approx 1.0$, and kiloparsec jets have $\alpha \approx 0.65$, while core dominated quasars generally have radio core spectral indices of $\alpha < 0.5$ (in the frequency band 1–5GHz). The spectral flux of the radio core typically turns over (steepens) between 50 and 250 GHz in the quasar rest frame [26, 27]. The radio emission from the flat spectrum radio core is often variable.

The spectral energy distribution, $\nu F_\nu$, of the radio core typically peaks in the mid-infrared [28]. The high frequency optical tail is steep spectrum, variable and polarized. Radio loud quasars, whether core or lobe dominated, seem to have broad emission line regions similar to those in radio quiet quasars. Furthermore, subtracting any optical/UV emission from the high energy tail of the core spectra yields spectra and luminosities similar to radio quiet quasars.

#### 1.3.1.4 Compact Radio Cores

There is also a panoply of compact radio sources (i.e., the total emission at 5 GHz is dominated by a "core" of radio emission that is radiated from a region less than 10 kpc across) that includes both flat and steep spectrum galaxies and quasars. The most common are compact steep spectrum quasars typically with emission on the order of 1 kpc in a twisted jet. Some of these objects have an inverted spectrum that peaks around 1 GHz and are referred to as "Gigahertz Peaked Radio Sources." Compact steep spectrum quasars rarely have significant emission on the scale of 100 kpc. The quasars 3C 286, 3C 287, and 3C 298 are well-known representatives of powerful, compact, steep spectrum objects with virtually no extended luminosity. The significant extended emission in 3C 380 is very unusual. Radio maps of compact steep spectrum cores can be found in [29] and a deep map of 3C 380 is published in [22].

Given sufficient resolution, a flat spectrum radio core usually can be found buried at the base of the jet within a steep spectrum radio core. This is consistent with a synchrotron radiation source of jet emission that becomes self-absorbed in the more compact inner regions. Every indication is that these sources have jets whose propagation is blocked by a dense intergalactic medium, or they are young radio sources with jets in the process of blasting out of the galaxy and will eventually become FR II radio sources.

#### 1.3.1.5 BL Lac Objects

BL Lac objects have strong flat spectrum radio cores and are extremely core dominated. However, they produce very weak signals of accretion phenomena. Their broad emission lines are intrinsically weaker than core dominated quasars. The optical luminosity is dominated by the high frequency tail of the radiation from the unresolved jet comprising the core. The optical luminosity is highly variable, steep spectrum, and polarized. Subtracting the optical/UV emission from the high frequency tail of the jet in a quiescent state of core emission leaves a residual luminosity too weak to be considered a quasar (i.e., the accretion disk luminosity is weak). BL Lac objects are more common at low redshift than core dominated quasars and the opposite is true at high redshifts.

#### 1.3.1.6 Unification

A deep connection between the various classes of objects emerged when the VLA (Very Large Array) was put into complete operation in the early 1980s. Many BL Lac objects were then shown to have diffuse halos in the high dynamic range VLA images at 1.4 GHz [21]. Later, it was shown even more conclusively that BL Lacs usually have a halo that resembles an FR I radio lobe viewed face on (i.e., same lobe luminosity and a morphology that is plume-like with no knots) [22, 30]. In fact, it was shown that most BL Lacs are FR I radio galaxies viewed along the axis of the jet [21]. The radio cores of BL Lacs reveal themselves in VLBI maps to be the relativistic subkiloparsec base of jets seen nearly end on and are therefore Doppler enhanced.

Similarly, the core dominated quasars are FR II quasars seen nearly end on (i.e., looking down the jet axis) [21, 22]. The radio core is the relativistic subkiloparsec scale jet approaching the earth. Furthermore, it was argued statistically that FR II radio galaxies are actually radio loud quasars in which the quasar emission is obscured by a surrounding dusty molecular torus [20] (see Fig. 1.9). This is supported by the morphological similarity of the radio galaxy Cygnus A (Fig. 1.7) and the quasar 3C 175 (Fig. 1.8). Often, the obscuring dusty molecular gas is assumed to have a toroidal distribution, but it need not be in such a symmetric, ordered configuration for the argument to hold. An equatorial obscuring torus is consistent with the fact that FR II radio galaxies have lower jet speeds than FR II quasar jets observed with the VLBI [31]. In the unified scheme, the jets in radio galaxies are more in the sky plane than the jets in quasars, and therefore they have lower Doppler factors. Direct evidence of obscured quasars in FR II radio galaxies is sparse as only a few objects show a hidden broad line region that is characteristic of a quasar in scattered (polarized) light.

One should note that the idea that radio loud quasars are physically distinct from radio quiet quasars is statistically robust. Efforts to construct a unified scheme in which radio loud quasars are just quasars seen from a preferred angle (i.e., pole on) assume all quasars are strong radio emitters. The fundamental flaw with this

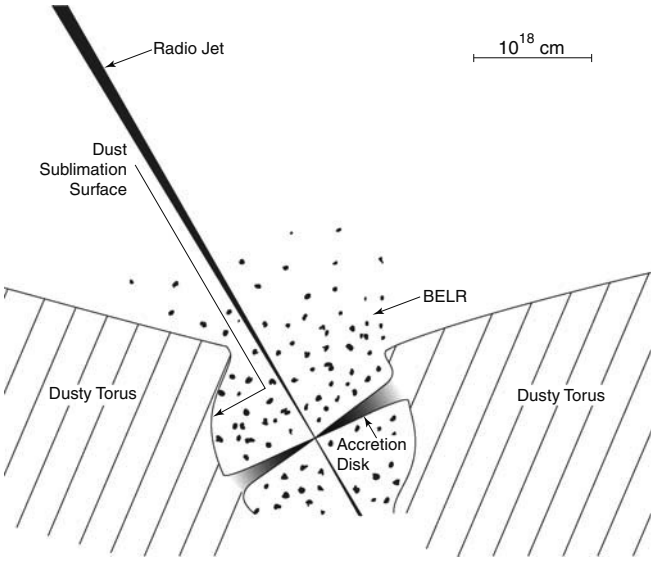


**Fig. 1.9** The "standard" unified model of FR II radio sources. An accretion disk orbits a central black hole with a fiducial mass of $10^9\,M_\odot$. The optical/UV emission can be obscured by a large scale distribution of dusty molecular gas (the dusty torus) for certain lines of sight; these objects are known as FR II radio galaxies. The broad emission line region (BELR) is a distribution of clouds that are photoionized by accretion disk radiation. The dusty torus also attenuates the BELR emission in FRII radio galaxies. By contrast, in FR II quasars the line of sight reveals both the accretion disk and the BELR. Core dominated radio loud quasars are viewed along lines of sight almost colinear with the radio jet axis

idea in that the radio lobe emission is at most mildly Doppler shifted (as exemplified by 3C 175 in Fig. 1.7). The lobe emission is essentially isotropic. When core dominated quasars are observed with high dynamic range, lobe emission is usually detected [22]. In this model, radio quiet quasars are those viewed off axis. Therefore, in a single quasar population model, we should usually see the isotropic lobe emission when a quasar is viewed off axis. Thus, most quasars should be (steep spectrum) radio loud on the basis of their extended structures. However, only $\sim$10% of quasars have detectable radio lobes. Furthermore, the distribution of radio luminosities in quasars is very close to being bimodal. Consequently the statistics of radio emissivity of quasars implied by such a unified scheme was shown to conflict strongly with observation [23].

#### 1.3.1.7 The Central Engine in the Unified Scheme

The unified scheme for extragalactic radio sources implies that the intrinsically weaker radio sources, FR I radio galaxies (or BL Lac objects when viewed end on), also have lower accretion rates (small thermal optical/UV emission). The most

luminous radio sources, quasars with FR II morphology (which appear as core dominated quasars when viewed end on, or FR II radio galaxies when viewed near the equatorial plane), are associated with large accretion rates. This is interesting in the context of black hole central engines (as accretion does not seem to power strong FR II radio emission in accord with the bimodal distribution of quasar radio luminosities noted above) as it implies that rapidly rotating black holes, spun up by rapid accretion, drive the most powerful jet/lobe emission in AGNs. This makes sense from a basic principle that the amount of reducible mass (extractable energy) scales with the rotational inertia of a black hole (see Sect. 1.4).

The physics of extragalactic radio source central engines is the primary motivation for studying black hole GHM. In general it is impossible to extract the rotational energy of a black hole in any type of reasonable physical process unless there is a black hole magnetosphere. The dynamics of such a magnetosphere are governed by GHM.

The numbers are suggestive of black hole rotation as a central engine as well. Take the example of the only nearby powerful FR II radio source, Cygnus A (to be discussed in detail in the next section). The data are still somewhat debatable as to whether a hidden quasar has been found [32]. The energy supplied to the lobes in particles and fields is on the order of $\gtrsim 10^{46}\,\mathrm{ergs\,s^{-1}}$, (see 1.23). Cygnus A emanates from a large elliptical galaxy as is typical of radio loud AGN. Dynamical estimates of central black hole masses in nearby weaker radio loud AGN in elliptical galaxies are typically $\sim 10^8 M_\odot$–$10^9 M_\odot$ (see Table 1.1). It will be shown in this monograph that electrodynamically $\sim 10\%$ of the mass–energy of a black hole is extractable. Thus, a black hole in an large elliptical galaxy could power Cygnus A for $\sim 10^8$ years, if it were initially rapidly rotating and a significant magnetosphere were present.

### *1.3.2 Quantifying the Power of Extragalactic Radio Sources*

In order to interpret the central engine in radio loud AGNs as supermassive black holes, one needs to quantify the power supplied to the extended radio structures. Although this is not a problem in relativistic astrophysics (as is the spirit of this book), it is of great significance for understanding the enormous power generated by the central engine and it is often not fully appreciated.

The power transported by the radio jets into the radio lobes usually far exceeds the radio luminosity. In this section, we describe the physical justification of this statement and estimate the power emitted by the central engine in Cygnus A. The observed synchrotron emission from the lobes requires both hot particles and magnetic fields. These particles and fields are advected outward as the lobes propagate into the intracluster medium and this is the dominant component of the energy supplied by the central engine. The ram pressure of the intracluster medium passing through the expanding boundary of the lobe is in balance with the internal pressure of the hot spot at the end of the lobe. This relation allows one to determine the lobe

advance speed if the density of the intracluster medium is known from X-ray observations. In turn, the size of the lobes, the internal pressures and lobe advance speed yield the kinematical power of the lobe.

The synchrotron spectral luminosity is a function of the magnetic field strength and the thermal energy spectrum of the radiating electrons. There is a component of energy density from both the magnetic field and the particles. A minimum value of the total energy for a given spectral luminosity can be estimated from the radio spectra and radio maps (which give the volume of the emitting region), $E_{min}$. Pressure balance near the hot spots in the lobes, yields the lobe advance speed and therefore the minimum energy flux supplied by the central engine, $Q_{min} = \mathrm{d}/\mathrm{d}t\, E_{min}$. When radio spectra, deep radio maps, and X-ray spectra are available, good estimates of $Q_{min}$ can be made, and such is the case for Cygnus A.

One can obtain an improved estimate of lobe energy compared to assuming a minimum energy plasma by studying the variation in the radio spectrum as a function of position within the lobe. This gradient in spectral index is known as "spectral aging." Spectral aging is a reference to the curvature that a power law spectrum attains over time because the high energy electrons radiate away their thermal energy faster than the low energy electrons. Thus, the high energy emission diminishes before the low energy emission causing a frequency dependent steepening (curvature) of the spectrum at high frequencies. Often the lobe advance speed disagrees with estimates derived from a spectral aging analysis that assumes a minimum energy configuration. The advantage of considering the spectral aging data in conjunction with X-ray observations of the intracluster medium is that it allows one to estimate how much the lobe energy exceeds the minimum energy value.

The power spectrum of a thermal electron gyrating in a magnetic field, $B$, simplifies for ultrarelativistic particles [33],

$$P(\nu) = \frac{4\sqrt{3}\pi}{3c} e^2 \gamma^{-2} \nu \int_{\nu/f_c}^{\infty} K_{5/3}(y)\, \mathrm{d}y \,\mathrm{ergs\,s^{-1}\,Hz^{-1}}; \tag{1.1}$$

where the electron cyclotron frequency is

$$\nu_B = \frac{eB}{2\pi m_e c}\,, \tag{1.2a}$$

the critical frequency is

$$f_c = (3/2)\,\nu_B \gamma^2, \tag{1.2b}$$

$K_{5/3}(y)$ is a modified Bessel function and $\gamma$ is the thermal Lorentz factor.

Consider a power law energy distribution of electrons in which the total number of electrons in the source $N_e$ is given by

$$N_e = \int\int N_0 \gamma^{-n}\, \mathrm{d}\gamma \mathrm{d}V\,. \tag{1.3}$$